 CMES, vol.74, no.3, pp.183-201, 2011

Application of An Atomistic Field Theory to Nano/Micro Materials Modeling and Simulation

Xiaowei Zeng[1]

Abstract: This paper presents an atomistic field theory and its application in modeling and simulation of nano/micro materials. Atomistic formulation and finite element implementation of the atomistic field theory is briefly introduced. Numerical simulations based on the field theory are performed to investigate the material behaviors of bcc iron at coarse-grained scale and we have obtained the mechanical strength and elastic modulus, which are in good agreement with results by first principles calculations. Also the nanoscale deformation and failure mechanism are revealed in bcc iron nanorods under simple tension. It is interesting to observe that under tensile loading, iron has gone through a bcc-fcc phase transformation before failure.

Keywords: Finite element; Molecular dynamics; Multiscale simulation; Nanorods; Phase transformation

1 Introduction

The last decades have seen exciting new developments in multiscale modeling approach, which has become a powerful simulation tool that may soon become a powerful research tool to supplement experimental and theoretical analysis in nanoscience and nano-technology. Conceptually, there are two categories of multiscale simulations: sequential multiscale simulations and concurrent multiscale simulations. The sequential multiscale methodology attempts to link different scales together through message passing mechanisms: large-scale models use the coarse-grained representations with information obtained from fine scale models. This sequential type of methods has proven effective in systems in which the different scales are weakly coupled. The general idea of the concurrent multiscale method is a paradigm that different scales are coexisting in a combined model, where different scales of the system communicate with each other through boundary message

[1] Department of Mechanical Engineering, University of Texas at San Antonio, TX 78249, USA, Corresponding Email: xiaowei.zeng@utsa.edu

passing e.g. hand-shaking procedures or permeable volume message passing. In a concurrent simulation, the system is often decomposed into domains characterized by different scales and physics. The different domains are treated by different methods; a successful multiscale model seeks a smooth coupling between these interfaces regions. This approach is mostly desirable for systems in which system behavior at each scale depends strongly on what happens at the other scales. Often times, concurrent multiscale simulations are employed to discover and to explain new and challenge physical phenomena.

There have been a number of reviews on multiscale simulation methods in the literature, with varying purposes and levels of details [Curtin and Miller (2003), Vvedensky (2004), Liu et al (2005), E and Li (2005), Lu and Kaxiras (2006), Miller and Tadmor (2009)]. Among various multiscale methods are the coupled length scale method [Abraham et al (1998a), Abraham et al (1998b), Rudd and Broughton (1998), Broughton et al (1999), Rudd and Broughton (2000)], the bridging scale method [Wagner and Liu (2003), Wagner et al (2004), Qian et al (2004), Karpov et al (2006), Park et al (2005)], the bridging domain method [Xiao and Belytschko (2004)], the mathematical homogenization theory [Chen and Fish (2006)], the perfectly matched method [To and Li (2005), Li et al (2006)], the Heterogeneous multiscale method [E and Engquist (2003), Li and E (2005)] and so forth. Another typical popular bottom up approach is the quasicontinuum method [Tadmor, Ortiz, Phillips (1996)], which is remarkably successful in many applications [Shenoy et al (1998), Miller et al (1998), Shenoy and Phillips (1999), Shenoy et al (1999), Tadmor et al (1999), Smith et al (2000), Smith et al (2001), Miller and Tadmor (2002), Tang et al (2006)]. It is also worthwhile to mention the recently developed multiresolution theory [Vernerey et al (2007), Vernerey et al (2008), McVeigh and Liu (2008), McVeigh and Liu (2009)], in which different length scales are built in the same framework.

An atomic based field theory has been initially proposed by Chen and Lee for concurrent atomic-continuum modeling of materials/systems [Chen and Lee (2005), Chen and Lee (2006)]. Further developments and applications of the field theory can be found in the following publications [Chen (2006), Chen et al (2006), Lei et al (2008), Chen (2009), Lee et al (2009a), Lee et al (2009b), Wang and Lee (2010), Zeng et al (2011), Wang et al (2011)]. In the theory, atomistic definitions and continuous local density functions of fundamental physical quantities are derived. By decomposing atomic motion/deformation into homogeneous lattice motion/deformation and inhomogeneous internal atomic motion/deformation, and also by decomposing momentum flux and heat flux into homogeneous and inhomogeneous parts, field description of conservation laws at atomic scale has been formulated. Since the conservation equations obtained by Chen et al. [Chen and

Lee (2005), Chen and Lee (2006)] are valid at atomic scale, the field theory can reproduce time-interval averaged atomic trajectories and can be used to investigate phenomena and properties that originated at atomic scale. On the other hand, it is a continuum field theory in terms of time-interval averaged quantities, and can be applied to simulate phenomena at larger length and time scales. A comparison of the atomistic field theory with classical continuum theory, the Micromorphic theory [Eringen and Suhubi (1964)], molecular dynamics simulations and quasicontinuum method can be found in Zeng et al. (2011).

2 Atomic Field Theory

Crystalline solids are distinguished from other states of matter by a periodic arrangement of the atoms; such a structure is called a crystal lattice. The atomic view of a crystal is as a periodic arrangement of local atomic bonding units. Each lattice point defines the location of the center of a unit. The space lattice is macroscopically homogeneous. Embedded in each lattice point is a group of bonded atoms, the smallest structural unit of the crystal. The structure of the unit together with the network of lattice points determines the crystal structure and hence the physical properties of the material.

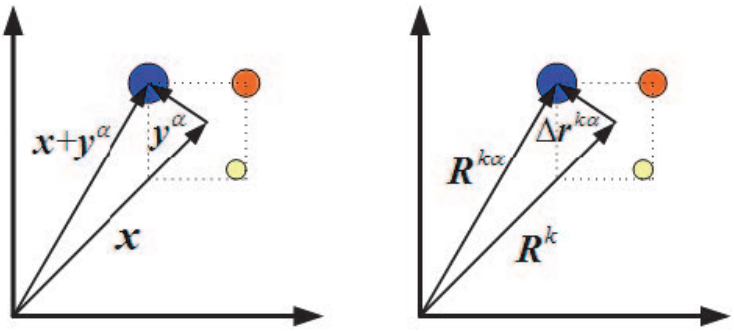

Figure 1: Description of deformation/motion decomposition in the field theory

Macroscopic quantities are generally described by continuous functions of physical space coordinates $\mathbf{x}$ and time t. They are fields in physical space-time. Microscopic dynamic quantities, on the other hand, are functions of phase-space coordinates $(\mathbf{r}, \mathbf{p})$, i.e., the positions and momenta of atoms. For multi-element systems, there

is more than one atom in a unit cell (see Figure 1). Thus, one has

$$\mathbf{r} = \left\{ \mathbf{R}^{k\alpha} = \mathbf{R}^k + \Delta\mathbf{r}^{k\alpha} \middle|\ k = 1,2,3,...n,\ \alpha = 1,2,3,..\upsilon \right\}$$
$$\mathbf{p} = \left\{ m^\alpha \mathbf{V}^{k\alpha} = m^\alpha \mathbf{V}^k + m^\alpha \Delta\mathbf{v}^{k\alpha} \middle|\ k = 1,2,3...n,\ \alpha = 1,2,3,...\upsilon \right\} \tag{1}$$

where the superscript $k\alpha$ refers to the $\alpha - th$ atom in the $k-th$ unit cell; n is the total number of unit cells in the system and υ is the number of atoms in a unit cell; m^α is the mass of the α-th atom; $\mathbf{R}^{k\alpha}$ and $\mathbf{V}^{k\alpha}$ are the position and velocity vector of the $k\alpha$ atom, respectively;$\mathbf{R}^k$ and $\mathbf{V}^k$ are the position and velocity of the mass center of the $k-th$ unit cell, respectively; $\Delta\mathbf{r}^{k\alpha}$ and $\Delta\mathbf{v}^{k\alpha}$ are the atomic position and velocity of the $\alpha - th$ atom relative to the mass center of the $k-th$ unit cell, respectively (see Figure 1). The local density of any measurable phase-space function $\mathbf{a}(\mathbf{r},\mathbf{p})$ can generally be defined as

$$\mathbf{A}(\mathbf{x},\mathbf{y}^\alpha,t) = \sum_{k=1}^{n} \sum_{\beta=1}^{\upsilon} \mathbf{a}\{\mathbf{r}(t),\mathbf{p}(t)\}\delta(\mathbf{R}^k - \mathbf{x})\tilde{\delta}(\Delta\mathbf{r}^{k\beta} - \mathbf{y}^\alpha) \equiv \mathbf{A}^\alpha(\mathbf{x},t) \tag{2}$$

The first delta function in eq. (2) is a localization function that provides the link between phase space and physical space descriptions. It can be a Dirac $\delta-$function by Irvine and Kirkwood (1950), or a distribution function by Hardy (1982), such as

$$\delta(\mathbf{R}^k - \mathbf{x}) = \pi^{-3/2} l^{-3} e^{-|\mathbf{R}^k - \mathbf{x}|/l^2} \tag{3}$$

The field descriptions of the conservation equations and the constitutive relations (the interrelations between field quantities) are found to be independent of the choices of the localization function [Chen and Lee (2005), Chen and Lee (2006)]. The second delta function in eq. (2) is a Kronecker delta, which identifies $\mathbf{y}^\alpha$ to $\Delta\mathbf{r}^{k\alpha}$. It can be easily proven that the following normalization condition holds

$$\int \delta(\mathbf{R}^k - \mathbf{x})\tilde{\delta}(\Delta\mathbf{r}^{k\alpha} - \mathbf{y}^\alpha) d^3\mathbf{x} = 1 \ (k = 1,2,3,...n)\ (\alpha = 1,2,..\upsilon) \tag{4}$$

Also, it is obvious that the distribution function, eq. (3), satisfies the following identity as the Dirac $\delta-$function does

$$\frac{\partial\delta(\mathbf{R}^k - \mathbf{x})}{\partial\mathbf{R}^k} = -\frac{\partial\delta(\mathbf{R}^k - \mathbf{x})}{\partial\mathbf{x}} \tag{5}$$

Physical properties, such as thermodynamic properties and transport properties, refer only to average behavior. Most current MD applications involve systems which

are either in equilibrium or in some time-independent stationary state; where individual results are subjected to fluctuation; it is the well-defined averages over sufficiently long time intervals that are of interest. In deriving the field description of atomic quantities and balance equations, it is the time-interval averaged quantities that are involved. The time-interval averaged (at time t in the interval $[t,\ t+\Delta t]$) local density function is defined as

$$\begin{aligned}\bar{\mathbf{A}}^{\alpha}(\mathbf{x},t) &= \langle \mathbf{A}^{\alpha}(\mathbf{x},t)\rangle \equiv \frac{1}{\Delta t}\int_{0}^{\Delta t}\mathbf{A}^{\alpha}(\mathbf{x},t+\tau)d\tau \\ &= \frac{1}{\Delta t}\int_{0}^{\Delta t}\sum_{k=1}^{n}\mathbf{a}\{\mathbf{r}(t+\tau),\mathbf{p}(t+\tau)\}\delta(\mathbf{R}^{k}-\mathbf{x})\tilde{\delta}(\Delta\mathbf{r}^{k\alpha}-\mathbf{y}^{\alpha})d\tau\end{aligned} \tag{6}$$

With the help of eq.(5), the time evolution of the local density function can be obtained as

$$\begin{aligned}\frac{\partial \mathbf{A}^{\alpha}}{\partial t}|_{\mathbf{x},\mathbf{y}^{\alpha}} &= \sum_{k=1}^{n}\frac{d\mathbf{a}}{dt}\delta(\mathbf{R}^{k}-\mathbf{x})\tilde{\delta}(\Delta\mathbf{r}^{k\alpha}-\mathbf{y}^{\alpha}) \\ &-\nabla_{\mathbf{x}}\cdot\left[\sum_{k=1}^{n}\mathbf{V}^{k}\otimes\mathbf{a}\delta(\mathbf{R}^{k}-\mathbf{x})\tilde{\delta}(\Delta\mathbf{r}^{k\alpha}-\mathbf{y}^{\alpha})\right] \\ &-\nabla_{\mathbf{y}^{\alpha}}\cdot\left[\sum_{k=1}^{n}\Delta\mathbf{v}^{k\alpha}\otimes\mathbf{a}\delta(\mathbf{R}^{k}-\mathbf{x})\tilde{\delta}(\Delta\mathbf{r}^{k\alpha}-\mathbf{y}^{\alpha})\right]\end{aligned} \tag{7}$$

When A^{α} is a conserved property, it results in a local conservation law that governs the time evolution of A^{α}. The mathematical representation of conservation equations for mass, linear momentum and energy at atomic scale has been analytically obtained in terms of averaged field quantities [Chen and Lee (2005), Chen and Lee (2006), Lee et al (2009a), Zeng et al (2011)], which are

$$\frac{d\bar{\rho}^{\alpha}}{dt}+\bar{\rho}^{\alpha}\nabla_{\mathbf{x}}\cdot\bar{\mathbf{v}}+\bar{\rho}^{\alpha}\nabla_{\mathbf{y}^{\alpha}}\cdot\Delta\bar{\mathbf{v}}^{\alpha}=0 \tag{8}$$

$$\bar{\rho}^{\alpha}\frac{d}{dt}(\bar{\mathbf{v}}+\Delta\bar{\mathbf{v}}^{\alpha})=\nabla_{\mathbf{x}}\cdot\bar{\mathbf{t}}^{\alpha}+\nabla_{\mathbf{y}^{\alpha}}\cdot\bar{\boldsymbol{\tau}}^{\alpha}+\bar{\boldsymbol{\phi}}^{\alpha} \tag{9}$$

where the time-interval averaged mass density$\bar{\rho}^{\alpha}$, linear momentum $\bar{\rho}^{\alpha}(\bar{\mathbf{v}}+\Delta\bar{\mathbf{v}}^{\alpha})$, homogeneous atomic stresses $\bar{\mathbf{t}}^{\alpha}_{(\mathrm{kin})}+\bar{\mathbf{t}}^{\alpha}_{(\mathrm{pot})}$ and inhomogeneous atomic stresses $\bar{\boldsymbol{\tau}}^{\alpha}_{(\mathrm{kin})}+\bar{\boldsymbol{\tau}}^{\alpha}_{(\mathrm{pot})}$, body force density $\bar{\boldsymbol{\phi}}^{\alpha}$ are defined as

$$\bar{\rho}^{\alpha}(\mathbf{x},t)\equiv\left\langle\sum_{k=1}^{n}m^{\alpha}\delta(\mathbf{R}^{k}-\mathbf{x})\tilde{\delta}(\Delta\mathbf{r}^{k\alpha}-\mathbf{y}^{\alpha})\right\rangle \tag{10}$$

$$\bar{\rho}^{\alpha}(\bar{\mathbf{v}}+\Delta\bar{\mathbf{v}}^{\alpha}) \equiv \left\langle \sum_{k=1}^{n} m^{\alpha}(\mathbf{V}^{k}+\Delta\mathbf{v}^{k\alpha})\delta(\mathbf{R}^{k}-\mathbf{x})\tilde{\delta}(\Delta\mathbf{r}^{k\alpha}-\mathbf{y}^{\alpha}) \right\rangle \tag{11}$$

$$\bar{\mathbf{t}}^{\alpha}_{(\mathrm{kin})} \equiv -\left\langle \sum_{k=1}^{n} m^{\alpha}\tilde{\mathbf{V}}^{k}\otimes\tilde{\mathbf{V}}^{k\alpha}\delta(\mathbf{R}^{k}-\mathbf{x})\tilde{\delta}(\Delta\mathbf{r}^{k\alpha}-\mathbf{y}^{\alpha}) \right\rangle \tag{12}$$

$$\bar{\boldsymbol{\tau}}^{\alpha}_{(\mathrm{kin})} \equiv -\left\langle \sum_{k=1}^{n} m^{\alpha}\Delta\tilde{\mathbf{v}}^{k\alpha}\otimes\tilde{\mathbf{V}}^{k\alpha}\delta(\mathbf{R}^{k}-\mathbf{x})\tilde{\delta}(\Delta\mathbf{r}^{k\alpha}-\mathbf{y}^{\alpha}) \right\rangle \tag{13}$$

$$\bar{\mathbf{t}}^{\alpha}_{(\mathrm{pot})} \equiv -\frac{1}{2}\left\langle \sum_{k,l=1}^{n}\sum_{\xi,\eta=1}^{\upsilon}(\mathbf{R}^{k}-\mathbf{R}^{l})\otimes\mathbf{F}^{k\xi}B(k,\xi,l,\eta,\mathbf{x},\mathbf{y}^{\alpha}) \right\rangle \tag{14}$$

$$\bar{\boldsymbol{\tau}}^{\alpha}_{(\mathrm{pot})} \equiv -\frac{1}{2}\left\langle \sum_{k,l=1}^{n}\sum_{\xi,\eta=1}^{\upsilon}(\Delta\mathbf{r}^{k\xi}-\Delta\mathbf{r}^{l\eta})\otimes\mathbf{F}^{k\xi}B(k,\xi,l,\eta,\mathbf{x},\mathbf{y}^{\alpha}) \right\rangle \tag{15}$$

$$\bar{\boldsymbol{\phi}}^{\alpha} \equiv \left\langle \sum_{k=1}^{n}\boldsymbol{\phi}^{k\alpha}\delta(\mathbf{R}^{k}-\mathbf{x})\tilde{\delta}(\Delta\mathbf{r}^{k\alpha}-\mathbf{y}^{\alpha}) \right\rangle \tag{16}$$

where $\mathbf{F}^{k\xi}$ is the interatomic force acting on the $k\xi$ atom; $\boldsymbol{\phi}^{k\alpha}$ is the body force acting the $k\alpha$ atom;

$$\tilde{\mathbf{V}}^{k\alpha} \equiv \mathbf{V}^{k\alpha}-\bar{\mathbf{v}}-\Delta\bar{\mathbf{v}}^{\alpha}\ ,\ \tilde{\mathbf{V}}^{k} \equiv \mathbf{V}^{k}-\bar{\mathbf{v}}\ ,\ \Delta\tilde{\mathbf{v}}^{k\alpha} \equiv \Delta\mathbf{v}^{k\alpha}-\Delta\bar{\mathbf{v}}^{\alpha} \tag{17}$$

$$B(k,\xi,l,\eta,\mathbf{x},\mathbf{y}^{\alpha}) \equiv \int_{0}^{1} d\lambda\,\delta\left(\mathbf{R}^{k}\lambda+\mathbf{R}^{l}(1-\lambda)-\mathbf{x}\right)\tilde{\delta}\left(\Delta\mathbf{r}^{k\xi}\lambda+\Delta\mathbf{r}^{l\eta}(1-\lambda)-\mathbf{y}^{\alpha}\right) \tag{18}$$

where $\bar{\mathbf{v}}$ is the time interval averaged velocity of the centroid of a unit cell and $\Delta\bar{\mathbf{v}}^{\alpha}$ is the time interval averaged velocity of the $\alpha-th$ atom relative to the centroid of the unit cell.

It is worthwhile to note that, with the atomistic definitions of interatomic force and the potential parts of the atomic stresses, one has

$$\nabla_{\mathbf{x}}\cdot\bar{\mathbf{t}}^{\alpha}_{(pot)}+\nabla_{\mathbf{y}^{\alpha}}\cdot\bar{\boldsymbol{\tau}}^{\alpha}_{(pot)} = \bar{\mathbf{f}}^{\alpha} \tag{19}$$

where $\bar{\mathbf{f}}^{\alpha}$ is the interatomic force density acting on the $\alpha-th$ atom in the unit cell located at $\mathbf{x}$.

3 Finite Element Formulation

In the finite element formulation, we work with time-interval averaged quantities. From now on, for simplicity, we drop the bars on top of the quantities if it does not cause ambiguity. The governing equations, eq.(9) can now be rewritten as

$$m^\alpha \ddot{\mathbf{u}}^\alpha = \{\nabla_{\mathbf{x}} \cdot \mathbf{t}^\alpha + \nabla_{\mathbf{y}^\alpha} \cdot \boldsymbol{\tau}^\alpha\} V + \mathbf{f}^\alpha + \boldsymbol{\phi}^\alpha \tag{20}$$

where $\mathbf{u}^\alpha$ is the displacement vector of the $\alpha - th$ atom; V is the volume of unit cell. We further assume that the temperature within a unit cell is uniform. This implies $T^\alpha = T(\mathbf{x},t)$ and $\nabla_{\mathbf{y}^\alpha} \cdot \boldsymbol{\tau}^\alpha = 0$. Now the governing equation, eq. (20), can be rewritten as [Lee et al (2009a), Zeng et al (2011)]

$$m^\alpha \ddot{\mathbf{u}}^\alpha = V \nabla \cdot \mathbf{t}^\alpha + \mathbf{f}^\alpha + \boldsymbol{\phi}^\alpha \tag{21}$$

with $t_{ij}^\alpha = -\gamma^\alpha k_B T \delta_{ij}/V$, $\tau_{ij}^\alpha = -(1-\gamma^\alpha) k_B T \delta_{ij}/V$ and $\gamma^\alpha \equiv m^\alpha / \sum_{\alpha=1}^{\nu} m^\alpha$. In this work, we are only concerned with 'one-way coupling' with temperature and electromagnetic fields, i.e., the temperature and electromagnetic fields are given as functions of space and time. Then the relevant governing equations are just the balance law for linear momentum:

$$m^\alpha \ddot{\mathbf{u}}^\alpha = -\gamma^\alpha k_B \nabla T + \mathbf{f}^\alpha + \boldsymbol{\phi}^\alpha \tag{22}$$

In case of temperature being constant, including $T = 0$, we can drop the first term in the right hand side of eq. (22), and the governing equation for any $\alpha - th$ atom in the $k - th$ unit cell can be rewritten as

$$m^\alpha \ddot{\mathbf{u}}(k,\alpha) = \mathbf{f}(k,\alpha) + \boldsymbol{\phi}(k,\alpha) \tag{23}$$

where $\mathbf{f}(k,\alpha)$ is all the interatomic force acting on the $\alpha - th$ atom in the $k - th$ unit cell; $\boldsymbol{\phi}(k,\alpha)$ is all the body force due to external field acting on the $\alpha - th$ atom in the $k - th$ unit cell. The effect of non zero temperature should be reflected in the boundary conditions. However, in this work we consider zero-temperature. Therefore, for a system with pair potential, one may rewrite eq. (23) as

$$m^\alpha \ddot{\mathbf{u}}(k,\alpha) = \sum_{l=1}^{n} \sum_{\beta=1}^{\upsilon} \mathbf{f}(k,\alpha\ ;\ l,\beta) + \boldsymbol{\phi}(k,\alpha) \tag{24}$$

where $\mathbf{f}(k,\alpha\ ;\ l,\beta)$ is the interatomic force acting on the $\alpha - th$ atom of the $k - th$ unit cell due to the interaction with the $\beta - th$ atom of the $l - th$ unit cell, with the

understanding $(k,\alpha) \neq (l,\beta)$. The inner product of eq. (24) with virtual displacement $\delta\mathbf{u}(k,\alpha)$ leads to

$$m^{\alpha}\ddot{\mathbf{u}}(k,\alpha)\cdot\delta\mathbf{u}(k,\alpha)=\sum_{l=1}^{n}\sum_{\beta=1}^{\upsilon}\mathbf{f}(k,\alpha\ ;\ l,\beta)\cdot\delta\mathbf{u}(k,\alpha)+\boldsymbol{\phi}(k,\alpha)\cdot\delta\mathbf{u}(k,\alpha) \tag{25}$$

Sum over all α and k, we obtain the following variational equation, the so-called weak form, as

$$\sum_{k=1}^{n}\sum_{\alpha=1}^{\upsilon}m^{\alpha}\ddot{\mathbf{u}}(k,\alpha)\cdot\delta\mathbf{u}(k,\alpha)=\sum_{k=1}^{n}\sum_{\alpha=1}^{\upsilon}\{\sum_{l=1}^{n}\sum_{\beta=1}^{\upsilon}\mathbf{f}(k,\alpha\ ;\ l,\beta)+\boldsymbol{\phi}(k,\alpha)\}\cdot\delta\mathbf{u}(k,\alpha) \tag{26}$$

Notice that eq. (26) can also be expressed as

$$\begin{aligned}\sum_{k=1}^{n}\sum_{\alpha=1}^{\upsilon}m^{\alpha}\ddot{\mathbf{u}}(k,\alpha)\cdot\delta\mathbf{u}(k,\alpha)&=\sum_{k=1}^{n}\sum_{\alpha=1}^{\upsilon}\sum_{l=1}^{n}\sum_{\beta=1}^{\upsilon}\mathbf{f}(l,\beta\ ;\ k,\alpha)\cdot\delta\mathbf{u}(l,\beta)\\&+\sum_{k=1}^{n}\sum_{\alpha=1}^{\upsilon}\phi(k,\alpha)\cdot\delta\mathbf{u}(k,\alpha)\end{aligned} \tag{27}$$

It is noticed that

$$\mathbf{f}(k,\alpha\ ;\ l,\beta)=-\mathbf{f}(l,\beta\ ;\ k,\alpha) \tag{28}$$

Therefore eq. (27) can be rewritten as

$$\begin{aligned}\sum_{k=1}^{n}\sum_{\alpha=1}^{\upsilon}m^{\alpha}\ddot{\mathbf{u}}(k,\alpha)\cdot\delta\mathbf{u}(k,\alpha)&=\frac{1}{2}\sum_{k=1}^{n}\sum_{\alpha=1}^{\upsilon}\sum_{l=1}^{n}\sum_{\beta=1}^{\upsilon}\mathbf{f}(k,\alpha\ ;\ l,\beta)\cdot[\delta\mathbf{u}(k,\alpha)-\delta\mathbf{u}(l,\beta)]\\&+\sum_{k=1}^{n}\sum_{\alpha=1}^{\upsilon}\phi(k,\alpha)\cdot\delta\mathbf{u}(k,\alpha)\end{aligned} \tag{29}$$

Suppose the whole specimen is divided into N_e finite elements ($8-node$ solid elements) with N_p finite elements nodes. Properly going through the process of nodal force assembly, the final FEM governing equation can be expressed as [Lee et al (2009a), Zeng et al (2011)]:

$$m^{\alpha}\ddot{\mathbf{u}}(I_p,\alpha)=\mathbf{F}(I_p,\alpha)+\boldsymbol{\phi}(I_p,\alpha)\ (I_p=1,2,3,....,N_p\ ;\ \alpha=1,2,3,....,\upsilon) \tag{30}$$

where $\mathbf{F}(I_p,\alpha)$ and $\boldsymbol{\phi}(I_p,\alpha)$ are the interatomic force and the body force acting on $\alpha-th$ atom of the I_p-th node, respectively. It is noticed that the mass matrix of eq. (30) is a diagonal matrix.

It is worthwhile to mention that in the atomistic field theory, both MD simulation and continuum modeling techniques can be utilized. Different meshes can be used in regions of different concerns, and if needed, mesh in critical region can be refined to the atomic scale, which is clearly described in eqs. (23, 30). Equation (23) is the basis for atomic simulation, since it is in terms of unit cells, while eq. (30) is the basis for finite element simulation, since it is in terms of finite element nodes. It has been proved that, when the element size reduces to the size of a unit cell, the field theory is automatically reduced to an atomic theory [Zeng et al (2011)].

4 Numerical Simulation

In this work, we first investigate the mechanical behavior in single crystal bcc iron under different mechanical loading conditions to obtain the material properties in coarse-grained models. The physical phenomena of bulging and necking are revealed by the simulation results. And then we reduced the element size to the size of a unit cell to study the mechanical deformation mechanism in bcc Fe nanorods. We observed the bcc-fcc phase transformation in bcc iron nanorods under simple tension. In these analyses, atomic units are used throughout unless otherwise explicitly specified.

4.1 Interatomic potential for Fe

In this work, we adopt the Finnis-Sinclair Model [Finnis and Sinclair (1984)] for material bcc iron. The potential energy of the Finnis-Sinclair Model (FSM) and the Embedded Atom Model (EAM) has the following general form:

$$U=\frac{1}{2}\sum_{i=1}^{N}\sum_{j=1}^{N}V_{ij}(r_{ij})+\sum_{i=1}^{N}F(\rho_i) \tag{31}$$

where $F(\rho_i)$ is a functional describing the energy of embedding, defined as

$$\rho_i=\sum_{j\neq i}^{N}\rho_{ij}(r_{ij})\ ,\ \mathbf{r}_{ij}\equiv\mathbf{r}_i-\mathbf{r}_j\ ,\ r_{ij}\equiv\left|\mathbf{r}_{ij}\right| \tag{32}$$

The Finnis-Sinclair potential is defined as

$$\begin{aligned} V_{ij} &= (r_{ij}-c)^2\left(c_0+c_1 r_{ij}+c_2 r_{ij}^2\right) \\ \rho_{ij}(r_{ij}) &= (r_{ij}-d)^2+\beta\frac{(r_{ij}-d)^3}{d} \\ F(\rho_i) &= -A\sqrt{\rho_i} \end{aligned} \tag{33}$$

with parameters $c_0, c_1, c_2, c, A, d, \beta$ from the reference [Finnis and Sinclair (1986)]; both c and d are cutoffs.

We rewrite the EAM/FSM potential as:

$$U = U_1 + U_2\ ,\ U_1 = \frac{1}{2}\sum_{i=1}^{N}\sum_{j=1}^{N} V_{ij}(r_{ij})\ ,\ U_2 = \sum_{i=1}^{N} F(\rho_i) \tag{34}$$

The atomic forces for FSM can be obtained as:

$$\mathbf{f}^k = -\frac{\partial U_1}{\partial \mathbf{r}_k} - \frac{\partial U_2}{\partial \mathbf{r}_k} \tag{35}$$

$$-\frac{\partial U_1}{\partial \mathbf{r}_k} = -\sum_{j=1, j\neq k}^{N}\left\{2\left(r_{kj}-c\right)\left(c_0+c_1 r_{kj}+c_2 r_{kj}^2\right)+\left(r_{kj}-c\right)^2\left(c_1+2c_2 r_{kj}\right)\right\}\frac{\mathbf{r}_{kj}}{r_{kj}} \tag{36}$$

$$-\frac{\partial U_2}{\partial \mathbf{r}_k} = \sum_{j=1, j\neq k}^{N}\frac{A}{2}\left(\frac{1}{\sqrt{\rho_k}}+\frac{1}{\sqrt{\rho_j}}\right)\left\{2\left(r_{kj}-d\right)+3\beta\frac{\left(r_{kj}-d\right)^2}{d}\right\}\frac{\mathbf{r}_{kj}}{r_{kj}} \tag{37}$$

4.2 Coarse-grained simulation of bcc iron

One approach to validate a theory and/or numerical implementation is to measure the elastic constant of a material. First principles calculations and experimental results occur in our simulation and essentially validate our theory and numerical implementation. The finite element model of the specimen for tension/shear test has $6\times 6\times 6$ finite elements; the total number of unit cells is 1,771,561. The stress-strain curves from tension and shear are shown in Fig.2 (a) and Fig.2 (b), respectively.

Figuratively speaking, the elastic modulus for single crystal bcc iron under small strain tension $\varepsilon = 0.02$ in the [0 0 1] direction is about 130 *GPa* which is in good agreement with the experimental value of 131 *GPa* through inelastic neutron scattering [Klotz and Braden (2000)] or 144 *GPa* through ultrasonic technique [Rayne

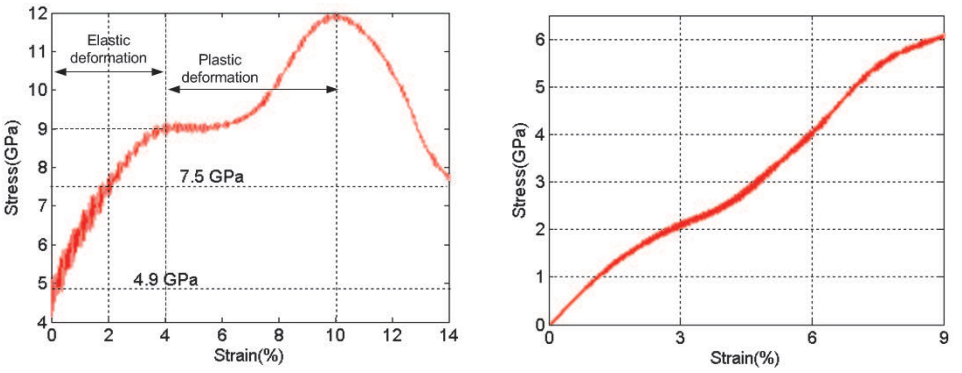

Figure 2: (a) Stress-strain curve of tension; (b) Stress-strain curve of shear

and Chandrasekhar (1961)]. Beyond the elastic limit, the stress-strain curve levels off and plastic deformation begins to occur. From Fig.2(a), we found the yield strength is about 9 *GPa* from the coarse-grained simulation. The tensile strength is about 11.9 *GPa* which is in reasonable agreement with the ideal strength of 12.6 *GPa* from first principle calculations [Clatterbuck et al (2003)]. The shear modulus is about 70 *GPa* which is in reasonable agreement with the experimental value of 78 *GPa* through ultrasonic technique [Leese and Load (1968)].

In this work, the single crystal bcc iron subjected to tensile and compressive loading conditions are simulated to show the necking and bulging phenomena. The finite element models of the specimen are shown in Fig.3 and Fig.4. The boundary conditions are the displacements specified at the two ends of the specimen as

$$u_z(x,y,0,t) = \begin{cases} -U^0 \times t/2t^0 & \text{if } t \le t^0 \\ -U^0/2 & \text{if } t^0 < t \le T \end{cases} \tag{38}$$

$$u_z(x,y,L,t) = \begin{cases} U^0 \times t/2t^0 & \text{if } t \le t^0 \\ U^0/2 & \text{if } t^0 < t \le T \end{cases} \tag{39}$$

where $U^0 = \varepsilon L$ with ε is the applied compressive or tensile strain; $t^0 = 0.8T$; T is the total simulation time.

Fig. 3 is the time evolution of the distribution of displacement u_z on deformed shape. The physical phenomenon of bulging is indeed revealed by the simulation results obtained. Similar to the case of compression, Fig. 4 shows the time evolution of the distribution of displacement u_z under tension. The snapshots show the material deforms gradually under constant strain rate. The simulation clearly shows

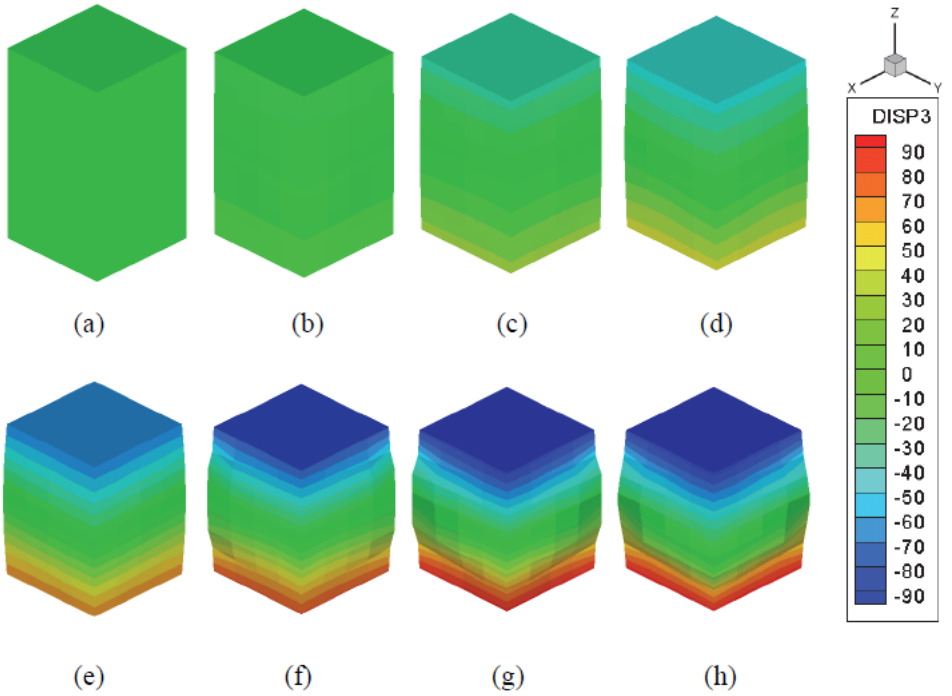

Figure 3: Time evolution of displacement (U_z) distribution on deformed shape under compression

the necking process, which demonstrates the atomistic field theory and its associated computer software are capable of dealing with large deformation problems. It is worthwhile to mention that continuum approximation is able to capture the overall failure mechanism. However it may predict different failure location other than molecular dynamics simulations since crystal structure under tensile loading involves material instability due to the failure evolution. To improve the accuracy, gradient terms can be developed in the field theory (see Vernerey et al ([2007], [2008]), McVeigh et al [2006], McVeigh and Liu [2009]).

4.3 Atomic Simulation of Bcc-fcc Phase Transformation

Nanorods have played an important role in the growing research field of multifunctional materials at the nanoscale, due to the interesting properties which emerge thanks to their finite size. They also exhibit a rich variety of structural transformations. Iron attracts additional interest due to the magnetism associated with the structural phase transition. In this work, the single crystal bcc iron nanorods

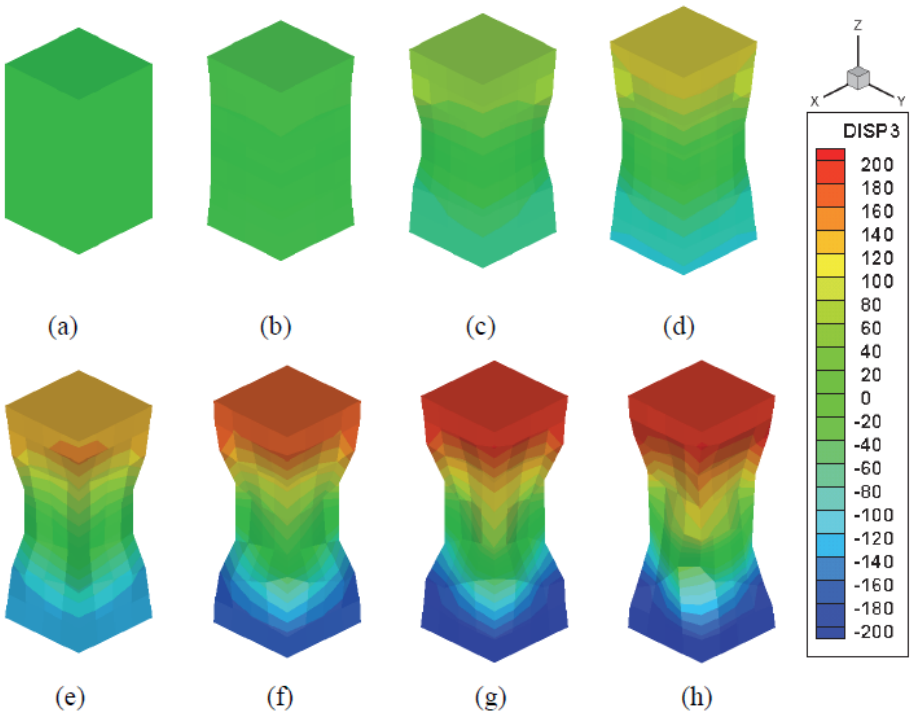

Figure 4: Time evolution of displacement (U_z) distribution on deformed shape under tension

subjected to tensile loading is studied by the formulated atomic field theory. The specimen consists of $5 \times 5 \times 10$ unit cells with 2 atoms per unit cell.

As shown in Figure 5, the dislocation planes were developed around one-third away from the bottom and top planes at strain $\varepsilon = 0.175$. The development of dislocation planes results in a crystal lattice transformation from a bcc structure to fcc structure at the dislocation interface. The initial lattice constant for bcc iron is $a = 2.87\overset{\circ}{A}$, we measure the lattice constant as $b = 3.50\overset{\circ}{A}$ after the bcc-fcc phase transformation. This transformation leads to crystal structure relaxation, whereby a portion of the crystal structure was displaced. The phase transformation from bcc to fcc for iron under uniaxial tension in [0 0 1] direction is reported by Clatterbuck et al (2003) from abinitio calculations. The dislocation necking was developed as the strain keeping increasing and finally the specimen fractured into two parts as shown in Figure 5.

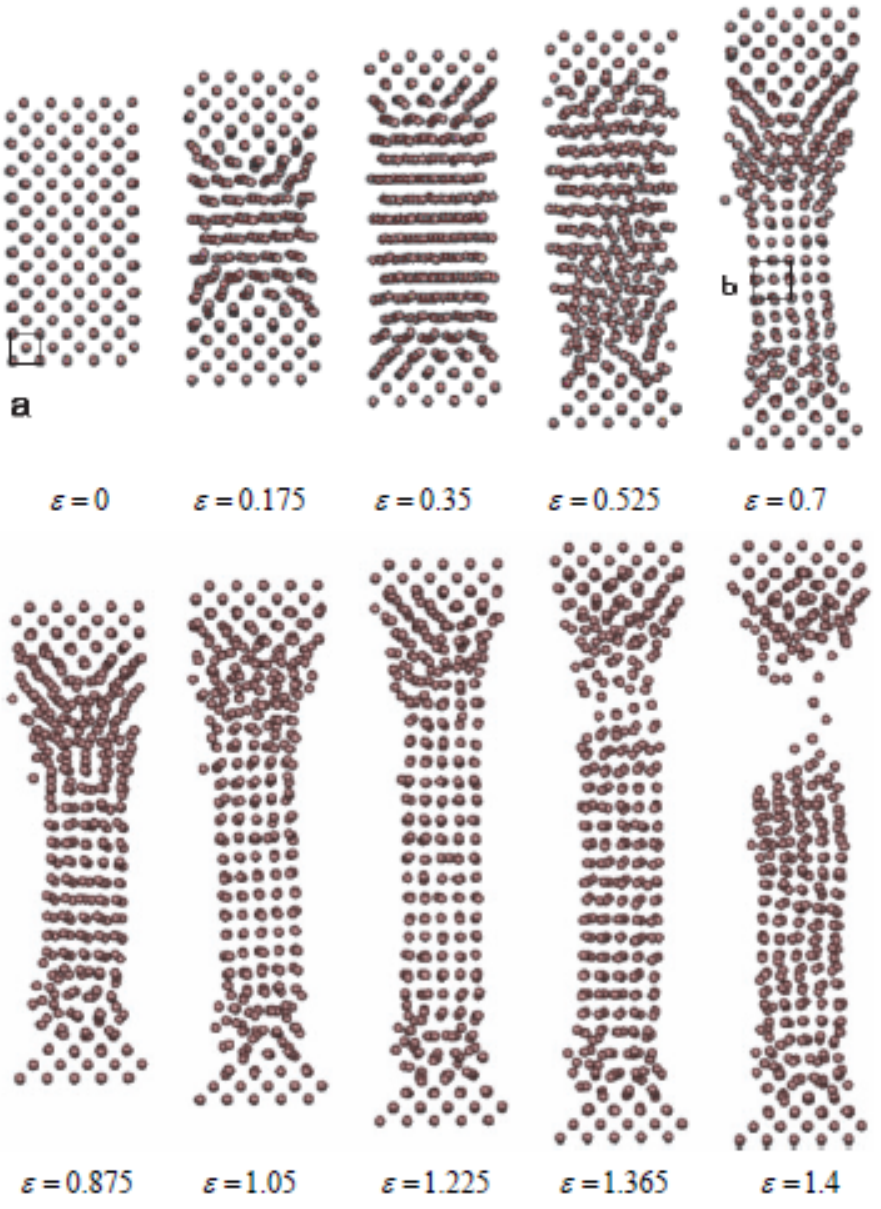

Figure 5: Crystal structure evolution during tensile loading

5 Summary

This paper presents an atomistic field theory and its application for coarse-grained and atomistic materials modeling and simulation. Numerical simulations based on the field theory are performed to investigate the material behaviors of bcc iron. The mechanism of deformation under different mechanical loading conditions is revealed. With the atomistic field theory, we have obtained the elastic properties of bcc iron, which are in good agreement with experimental data or first principle calculations. We observed the bcc-fcc phase transformation in bcc iron nanorods under simple tension. It has been shown that the atomic based field theory can work both on atomic-scale and macro-scale. It has been proven that, when the element size reduces to the size of a unit cell, the field theory is automatically reduced to an atomic theory. This thus naturally leads to a concurrent atomic/continuum model without the need for scale decoupling or a region of hand-shaking. Therefore the filed theory has the capability to work as a predictive materials research tool to understand the structure and properties of materials at different scales.

Acknowledgement: The support to this work by National Science Foundation under Award Numbers CMS-0301539 and CMS-0428419 is gratefully acknowledged.

References

Abraham, F. F.; Broughton, J. Q.; Bernstein, N.; Kaxiras, E. (1998a): Spanning the continuum to quantum length scales in a dynamic simulation of brittle fracture, *Europhys. Lett.* 44, 783-787.

Abraham, F. F.; Broughton, J. Q.; Bernstein, N.; Kaxiras, E. (1998b): Spanning the length scales in dynamic simulation, *Computers in Phys.* 12, 538-546.

Broughton, J. Q.; Bernstein, N.; Kaxiras, E.; Abraham, F. F. (1999): Concurrent coupling of length scales: Methodology and application, *Physical Review B* 60, 2391-2403.

Chen, W.; Fish, J. (2006): A generalized space-time mathematical homogenization theory for bridging atomistic and continuum scales, *Int. J. Numer. Methods Eng.* 67, 253–271.

Chen, Y.; Lee, J. D. (2005): Atomistic formulation of a multiscale theory for nano/micro physics, *Philosophical Magazine* **85**, 4095-4126.

Chen, Y.; Lee, J. D. (2006): Conservation laws at nano/micro scales, *Journal of Mechanics of Materials and Structures* 1, 681-704.

Chen, Y. (2006), Local stress and heat flux in atomistic systems involving three-

body forces, *Journal of Chemical Physics* 124, 054113.

Chen, Y.; Lee, J. D.; Xiong, L. (2006): Stresses and strains at nano/micro scales, *Journal of Mechanics of Materials and Structures* 1, 705-723.

Chen, Y. (2009): Reformulation of microscopic balance equations for multiscale materials modeling, *J. Chem. Phys*. 130(13), 134706.

Clatterbuck, D.M.; Chrzan, D. C.; Morris, Jr. J.W. (2003): The ideal strength of iron in tension and shear, *Acta Material* 51, 2271-2283.

Curtin, W. A.; Miller, R. E. (2003): Atomistic/continuum Coupling in Computational Materials Science, *Modeling and Simulation in Materials Science and Engineering*, 11, 33–68.

E, W.; Engquist, B. (2003): The Heterogeneous multi-scale methods, *Comm. Math. Sci*. 1(1), 87-132.

E, W.; Li, X. T. (2005): Multiscale Modeling for crystalline solids, *Handbook of multiscale material modeling*, Ed. Sidney Yip, Springer, NY.

Eringen, A. C.; Suhubi, E.S. (1964): Nonlinear theory of simple microelastic solids-I. Int J Eng Sci 2:189–203

Finnis, M. W.; Sinclair, J. E. (1984): A simple empirical N-body potential for transition metals, *Philosophical Magazine A* 50 (1), 45-55.

Finnis, M. W.; Sinclair, J. E. (1986): Erratum: A simple empirical N-body potential for transition metals, *Philosophical Magazine A* 53 (1), 161.

Hardy, R. J. (1982): Formulas for determining local properties in molecular-dynamics simulations: Shock waves, *J. Chem. Phys.* 76 (1), 622-628.

Irvine, J. H.; Kirkwood, J. G. (1950): The statistical theory of transport processes. IV. The equations of hydrodynamics, *J. Chem. Phys.* 18, 817-829.

Karpov, E. G.; Yu, H.; Park, H. S.; Liu, W. K.; Wang, J.; Qian, D. (2006): Multiscale boundary conditions in crystalline solids: Theory and application to nanoindentation, *International Journal of Solids and Structures*, 43(21), 6359-6379.

Klotz, S.; Braden, M. (2000): Phonon dispersion of bcc iron to 10 GPa, *Phys. Rev. Lett*. **85,** 3209-3212.

Lee, J. D.; Wang, X.; Chen, Y. (2009a): Multiscale material modeling and its application to a dynamic crack propagation problem, *Theoretical and Applied Fracture Mechanics*, 51, 33-40.

Lee, J. D.; Wang, X.; Chen, Y. (2009b): Multiscale computational for nano/micro material. *Journal of Engineering Mechanics*, 135, 192-202.

Leese, J.; Load, Jr. A. E. (1968): Elastic stiffness coefficients of single-crystal iron from room temperature to 500^0C, *Journal of Applied Physics* 39, 3986-3988.

Lei, Y.; Lee, J. D.; Zeng, X. (2008): Response of a rocksalt crystal to electromagnetic wave modeled by a multiscale field theory, *Interaction and Multiscale Mechanics* 1(4), 467-476.

Li, S.; Liu, X.; Agrawal, A.; To, A. C. (2006): Perfectly matched multiscale simulations for discrete systems: Extension to multiple dimensions, *Physical Review B* 74, 045418.

Li, X. T.; E, W. (2005): Multiscale modeling of dynamics of solids at finite temperature, *J. Mech. Phys. Solids,* 53, 1650-1685.

Liu, W. K.; Jun, S.; Qian, D. (2005): Computational Nanomechanics of Materials, Handbook of Theoretical and Computational Nanotechnology, Eds. M. Rieth and W. Schommers, American Scientific Publishers, Stevension Ranch, CA.

Lu, G.; Kaxiras, E. (2006): Overview of Multiscale Simulations of Materials, *Handbook of Theoretical and Computational Nanotechnology*, Eds. Michael Rieth and Wolframe Schommers, American Scientific Publishers, Volume X, pp. 1-33.

McVeigh, C.; Liu, W. K. (2008): Linking microstructure and properties through a predictive multiresolution continuum, *Comput. Methods Appl. Mech. Engrg.* 197: 3268–3290.

McVeigh, C.; Liu, W. K. (2009): Multiresolution modeling of ductile reinforced brittle composites, *J. Mech. Phys. Solids* 57: 244-267.

Miller, R. E.; Tadmor, E. B.; Phillips, R.; Ortiz, M. (1998): Quasicontinuum simulation of fracture at the atomic scale, *Model. Simul. Mater. Sci. Eng.*, 6, 607-638.

Miller, R. E.; Tadmor, E. B. (2002): The Quasicontinuum method: overview, applications and current directions, *Journal of Computer-Aided Materials Design*, 9(3), 203-239.

Miller, R. E.; Tadmor, E. B. (2009): A unified framework and performance benchmark of fourteen multiscale atomistic/continuum coupling methods, *Modelling Simul. Mater. Sci. Eng.* 17 053001.

Park, H. S.; Karpov, E. G.; Liu, W. K.; Klein, P. A. (2005): The bridging scale for three-dimensional atomistic/continuum coupling, *Philosophical Magazine* 85(1), 79-113.

Qian, D.; Wagner, G. J.; Liu, W. K. (2004): A multiscale projection method for the analysis of carbon nanotubes, *Computer Methods in Applied Mechanics and Engineering*, 193, 1603-1632.

Rayne, J. A.; Chandrasekhar, B. S. (1961): Elastic constants of iron from 4.2 to 300K, *Phys. Rev*. 122, 1714-1716.

Rudd, R. E.; Broughton, J. Q. (1998): Coarse-grained molecular dynamics and

atomic limit of finite elements, *Physical Review B* 58, 5893-5896.

Rudd, R. E.; Broughton, J. Q. (2000): Concurrent coupling of length scales in solid state systems, *Phys. Stat. Sol.* **217,** 251-291.

Shenoy, V. B.; Miller, R.; Tadmor, E. B.; Phillips, R.; Ortiz., M. (1998): Quasicontinuum models of interfacial structure and deformation, Phys. Rev. Lett., 80, 742-745.

Shenoy, V.; Phillips, R. (1999): Finite temperature quasicontinuum methods, *Mat. Res. Soc. Symp. Proc.,* 538, 465-471.

Shenoy, V. B.; Miller, R.; Tadmor, E. B.; Rodney, D.; Phillips, R.; Ortiz, M. (1999): An adaptive finite element approach to atomic-scale mechanics-the quasicontinuum method, *J. Mech. Phys. Solid*, 47, 611-642.

Smith, G. S.; Tadmor, E. B.; Kaxiras, E. (2000): Multiscale simulation of loading and electrical resistance in silicon nanoindentation, Phys. Rev. Lett., 84, 1260-1263.

Smith, G. S.; Tadmor, E. B.; Bernstein, N.; Kaxiras, E. (2001): Multiscale simulations of silicon nanoindentation, *Acta Mater.*, 49, 4089-4101.

Tadmor, E. B.; Ortiz, M.; Phillips, R. (1996): Quasicontinuum analysis of defects in solids, Phil. Mag. A 73, 1529–63

Tadmor, E. B.; Miller, R.; Phillips, R.; Ortiz, M. (1999): Nanoindentation and incipient plasticity, *J. Mater. Res.*, 14, 2233-2250.

Tang, Z.; Zhao, H.; Li, G.; Aluru, N. R. (2006): Finite temperature quasicontinuum method for multiscale analysis of silicon nanostructures, *Phys. Rev. B*, 74, 064110.

To, A. C.; Li, S. (2005): Perfectly matched multiscale simulations, *Physical Review B* 72, 035414.

Vernerey, F. J.; Liu, W. K.; Moran, B. (2007): Multi-scale Micromorphic theory for hierarchical materials, *Journal of the Mechanics and Physics of Solid* 55(12): 2603-2651.

Vernerey, F. J.; Liu, W. K.; Moran, B.; Olson, G. B. (2008): A micromorphic model for the multiple scale failure of heterogeneous materials, *Journal of the Mechanics and Physics of solids* 56(4): 1320-1347.

Vvedensky, D. D. (2004): Multiscale Modeling of Nanostructures, *Journal of Physics: Condensed Matter*, 16, 1537–1576.

Wagner, G. J.; Liu, W. K. (2003): Coupling of atomic and continuum simulations using a bridging scale decomposition, *J. Comput. Phys.* 190, 249-274.

Wagner, G. J.; Karpov, E. G.; Liu, W. K. (2004): Molecular dynamics boundary

conditions for regular crystal lattices, *Computer Methods in Applied Mechanics and Engineering*, 193(17-20), 1579-1601.

Wang, X. and Lee, J. D. (2010), An atom-based continuum method for multi-element crystals at nano-scale, *Computer Modeling in Engineering & Sciences* 69(3):199-222.

Wang, X; Lee, J. D.; Deng, Q. (2011), Modeling and simulation of wave propagation by Atomistic Field Theory, *ASME Journal of Applied Mechanics* 78, 021012.

Xiao, S. P.; Belytschko, T. (2004): A bridging domain method for coupling continua with molecular dynamics, *Comput. Methods Appl. Mech. Eng.* 193, 1645–1669.

Zeng, X.; Wang, X.; Lee, J. D.; Lei, Y. (2011): Multiscale modeling of nano/micro systems by a multiscale continuum field theory, *Computational Mechanics,* 47, 205-216.